ACS APPLIED MATERIALS & INTERFACES

RESEARCH ARTICLE

www.acsami.org

Surfactant Effects on Efficiency Enhancement of Infrared-to-Visible Upconversion Emissions of $NaYF_4$:Yb-Er

Mei Chee Tan, Lara Al-Baroudi, and Richard E. Riman*

Department of Materials Science and Engineering, Rutgers, The State University of New Jersey, 607 Taylor Road, Piscataway, New Jersey 08854, United States

ABSTRACT: Infrared-to-visible rare earth doped upconversion phosphors that convert multiple photons of lower energy to higher energy photons offer a wide range of technological applications. The brightness (i.e., emission intensities) and energy efficiency of phosphors are important performance characteristics that determine which applications are appropriate. Optical efficiency can be used as a measure of the upconversion emission performance of these rare earth doped phosphors. In this work, hexagonal-phase $NaYF_4$:Yb-Er was synthesized using the hydrothermal method in the presence of surfactants like trioctylphosphine, polyethylene glycol monooleate, and polyvinylpyrrolidone. The upconversion emission optical efficiencies of $NaYF_4$:Yb-Er were measured to quantify and evaluate the effects of surface coatings and accurately reflect the brightness and energy efficiency of these phosphors. Polyvinylpyrrolidone-modified $NaYF_4$:Yb-Er particles were found to be ~5 times more efficient and brighter than the unmodified particles. The difference in efficiency was attributed to reduced reflectance losses at the particle−air interface via refractive index mismatch reduction between the core $NaYF_4$:Yb-Er particles and air using polyvinylpyrrolidone as a surfactant.

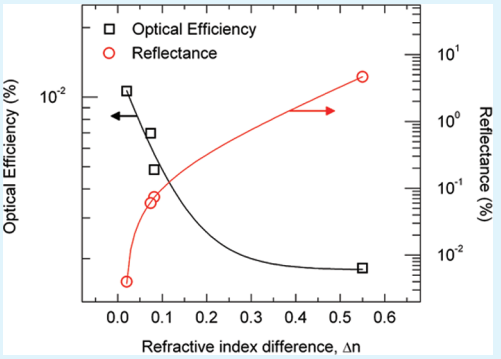

KEYWORDS: luminescence, phosphors, surface modification, optical efficiency, upconversion, rare-earth-doped materials

1. INTRODUCTION

Infrared-to-visible rare earth doped upconversion phosphors that convert multiple photons of lower energy to higher energy photons offer a wide range of technological applications in solid-state lasers, three-dimensional flat-panel displays, energy-efficient photovoltaic devices, biomedical imaging, and photodynamic therapy applications.[1−6] The absorption and emission properties of rare-earth doped materials can be tailored by controlling the local environment, such as site symmetry, crystal field strength, and electron−phonon interaction strength of rare-earth dopants. Halide hosts (e.g., $NaYF_4$, YF_3, CaF_2, LaF_3) are favored for their low phonon energies which minimize non-radiative losses to enable intense infared-to-visible up-converting emissions.[7−10] Among the various fluoride hosts, low phonon energy hexagonal-phase $NaYF_4$, doped with either Yb-Er or Yb-Tm trivalent rare earth ions, is recognized as one of the most efficient hosts for the infrared-to-visible upconversion process.[9,11] Besides the low phonon energy host, the high upconversion efficiency has been attributed to the multisite character of the hexagonal-phase $NaYF_4$ crystal lattice, where the rare earth active center may occupy two or three non-equivalent sites.[12,13] Yb^{3+} ions are added to serve as a sensitizer that enhances the infrared-to-visible upconversion efficiency due to the strong energy transfer from Yb^{3+} to neighboring Er^{3+} (or Tm^{3+}) ions.

In most cases, brightness (i.e., emission intensities) and energy efficiency are used as measures of the phosphor performance. The brightness and energy efficiency of phosphors are important performance characteristics that determine which applications are appropriate. For example, brighter and more efficient phosphors improve the diagnostic sensitivity of biomedical phosphor probes and enhance the energy efficiency of phosphor-based illuminators. Radiant efficiency, the ratio of emitted power to absorbed power, was used to measure the emission intensity and brightness of the different upconversion phosphors.[14,15] Efficiencies in the range of 10^{-3} to 10^{-4} were reported for most upconversion phosphors. However, the approach for evaluation of phosphor performance leads to significant measurement errors. The relatively low rare earth concentrations (<2 mol %) leads to low absorption cross sections (typically of the order from 1×10^{-21} to 5×10^{-20} cm^2). Low absorption in conjunction with scattering and reabsorption losses are not properly accounted for in computing radiant efficiency. Since optical efficiency is the ratio of emitted power to incident power, this approach circumvents the absorption measurement related errors. Recently, we have demonstrated that optical efficiency can be used as a measure of the upconversion emission performance of rare earth doped phosphors.[16]

There has not been a study that has examined the influence of surfactants and surface coatings on optical efficiency of infrared-to-visible upconversion rare earth doped phosphor microparticles. Surfactants, surface-active agents, are often added to control particle size and particle morphology, as well as modulate the

Received: June 14, 2011
Accepted: August 26, 2011
Published: August 26, 2011

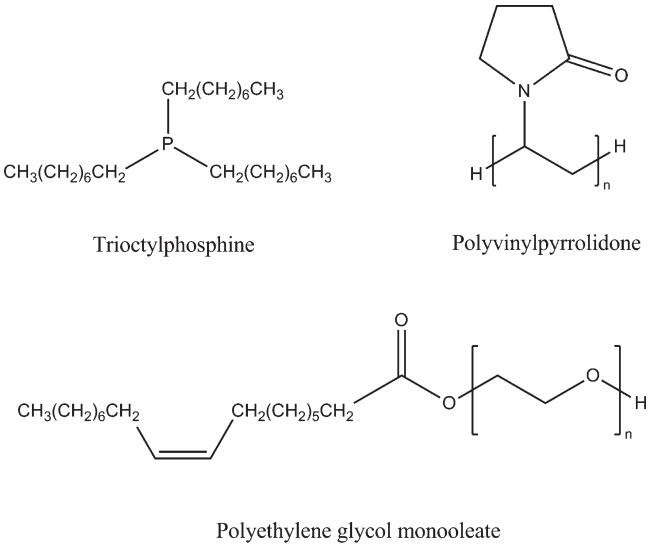

Figure 1. Molecular structure of surface capping agents used for hydrothermal synthesis of hexagonal-phase $NaYF_4$:Yb-Er.

dispersion of these particles.[17−19] These surfactants are expected to affect optical performance and efficiency by attenuating either the excitation or emission light. The alkyl ($-CH_2$) and hydroxyl ($-OH$) groups on surfactants have been reported to deactivate surface rare earth ions and quench any emissions from nanoparticles.[7,20,21] The contribution of surface quenching effects from these surfactants is minimized using larger micrometer-sized particles where the percentage of surface atoms per particle ($\ll$10%) is negligible. In this work, hexagonal-phase $NaYF_4$:Yb-Er was synthesized in the presence of three different surfactants, trioctylphosphine, polyethylene glycol monooleate (PEG monooleate), and polyvinylpyrrolidone, using the hydrothermal method. The molecular structures of each of these surfactants are shown in Figure 1 and are known to physisorb on the surfaces of a wide range of particles.[22−27] The optical efficiencies of the upconversion emissions for surface-modified $NaYF_4$:Yb-Er were measured to quantitatively evaluate the effects of surfactants on the brightness and energy efficiency of these phosphors.

2. EXPERIMENTAL METHODS

2.1. Hydrothermal Synthesis of $NaYF_4$:Yb-Er Upconversion Phosphors. Stoichiometric amounts of rare earth nitrates (Sigma Aldrich, St. Louis, MO) were mixed with 1.5 times excess sodium fluoride in ~70 mL of water/ethanol mixture (80:20 v/v) and various additives for 30 min to synthesize $NaY_{0.78}Yb_{0.20}Er_{0.02}F_4$ particles. No organic additives were added to the reaction mixture for the synthesis of unmodified particles. 2×10^{-4} moles which corresponds to 0.1 mL, 0.1 mL, and 8 g of trioctylphosphine, polyethylene glycol monooleate (PEG monooleate, average $M_n \sim 460$ g/mol), and polyvinylpyrrolidone (average $M_n \sim 40\,000$ g/mol), respectively, from Sigma Aldrich was added to the reaction mix. This mixture was next transferred to a 125 mL Teflon liner and heated to ~240 °C for 4 h in a Parr pressure vessel (Parr Instrument Company, Moline, IL). The as-synthesized particles were washed three times in deionized water by centrifuging (Beckman-Coulter Avanti J-26 XP, Fullerton, CA) and dried at 70 °C in air in a mechanical convection oven (Thermo Scientific Thermolyne, Waltham, MA) for further powder characterization.

2.2. Powder Characterization. Scanning electron microscopy (SEM) images of the powder samples were taken using the Carl Zeiss Σigma field emission scanning electron microscope (Carl Zeiss, Carl Zeiss SMT Inc., Peabody, MA) using the secondary electron detector and operating at an accelerating voltage of 5.0 kV with a working distance of 10 mm. Primary particle sizes and aspect ratios from SEM micrographs were evaluated using digital image processing and analysis software, IMAGEJ.[28] Particle morphology was poorly fitted to a rectangle using IMAGEJ software. However, the results generated using IMAGEJ by fitting particle area to a rectangle shape were sufficient to give a qualitative determination of particle morphology changes. Results generated from the software were manually verified by selecting and measuring approximately ten random particles from each micrograph. Energy-dispersive X-ray (EDX) spectroscopy area scans of the powder samples were also completed to determine its elemental composition by increasing the accelerating voltage to 25 kV and reducing the working distance to 8.5 mm for an aperture of 30 μm. The EDX elemental composition was determined by comparing relative peak intensities together with the corresponding sensitivity factors of each element and assuming their total intensities to be 100%.

Powder X-ray diffraction (XRD) patterns were obtained with a resolution of 0.04°/step and 2 s/step with the Siemens D500 (Bruker AXS Inc., Madison, WI) powder diffractometer (40 kV, 30 mA), using Cu Kα radiation (λ = 1.54 Å). Powder diffraction files (PDF) from International Centre for Diffraction Data (ICDD, Newtown Square, PA) PDF#97-005-1917 for hexagonal $NaYF_4$ were used as reference.

X-ray photoelectron spectroscopy (XPS) measurements were performed using XSAM 800 KRATOS apparatus with a 127 mm radius concentric hemispherical analyzer (CHA). An Al Kα radiation with a photon energy of 1486.6 eV was used as X-ray source; and photoelectrons were detected by the CHA operated in the fixed retarding ratio mode FRR5 (survey scans) and in the fixed analyzer transmission modes FAT20 or FAT40 (detail scans) with pass energies of 20 and 40 eV, respectively. XPS quantification of the atomic fraction for each component was determined by comparing relative intensities of photoelectron peaks together with the corresponding sensitivity factors and assuming their total intensities to be 100%. The atomic fraction was subsequently normalized to the integrated intensity of Na (2s) peaks to allow for comparisons between samples. The measurements were performed under UHV conditions with a residual pressure of about 10^{-9} Torr. For destructive depth profiling, etching of powder samples was conducted by sputtering in an Ar atmosphere at 3 keV and 3 $\mu A/cm^2$ for 15 min.

The phosphor powder samples were packed in demountable Spectrosil far UV quartz Type 20 cells (Starna Cells, Inc., Atascadero, CA) with 0.5 mm path lengths for optical emission measurements. The optical emission spectra of nanoparticles excited at ~976 nm with a 2.5 W laser (BW976, BW Tek, Newark, NJ) were collected using the FSP920 Edinburgh Instruments spectrometer (Edinburgh Instruments, Livingston, United Kingdom) that was equipped with a Hamamatsu R928P photomultiplier tube detector.

For the optical efficiency measurements, powder samples of as-prepared phosphors were dry pressed into pellets of 1 cm diameter and 2 mm thickness.[16] A modification of the C9220-03 quantum yield measurement system from Hamamatsu (Hamamatsu, Bridgewater, NJ) was used to make the optical efficiency measurements. In brief, the measurement principle is based on direct illumination and indirect reflection. Light enters the integrating sphere through the sample port, goes through multiple reflections, and is scattered uniformly around the interior of the sphere. For our measurements, the integrating sphere was set up in the reflectance mode to measure total integrated reflectance of a surface. The PD300-IR and PD300-UV power detectors (Ophir-Spiricon, Logan, UT) which measure the power of emitted light were used in place of the photomultiplier tube that was originally on the C9220-03 quantum yield measurement system. They were positioned at the port at the side of the sphere where the emitted beam is independent of the angular properties of light at the sample port. A further assumption made during

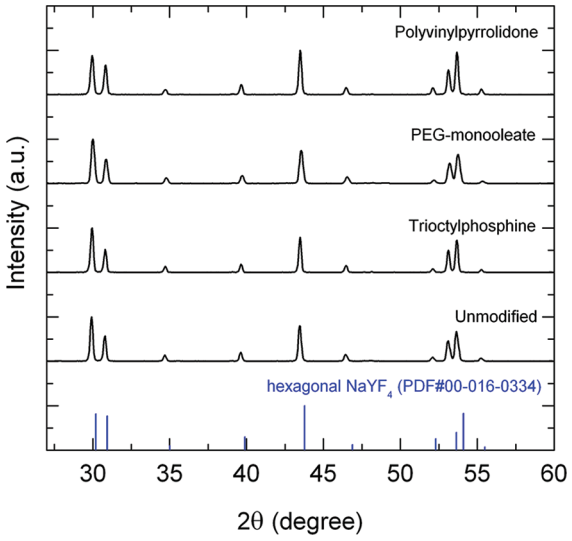

Figure 2. XRD profiles of $NaYF_4$:Yb-Er particles synthesized with different surface capping agents compared with the unmodified particles.

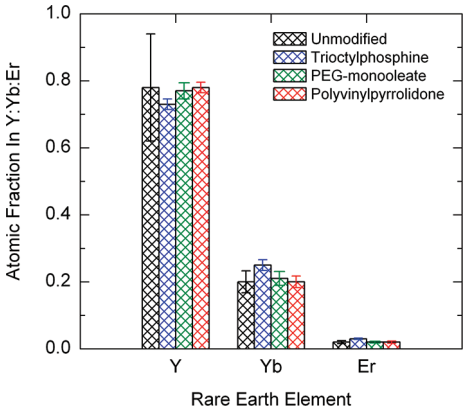

Figure 3. EDX-based elemental composition of $NaYF_4$:Yb-Er particles synthesized using different surface capping agents compared with the unmodified particles.

measurements is that all light emanating from the different samples is isotropic.

3. RESULTS AND DISCUSSION

From the XRD profiles as shown in Figure 2, pure hexagonal-phase $NaYF_4$:Yb-Er powders were synthesized using the hydrothermal method and different surfactants. No statistically significant differences in crystallite sizes were observed on the basis of the full width at half-maximum of the various diffraction peaks for the different powders. Using the Scherrer equation, the average crystallite size estimated for each of the different powders shown in Figure 2 was ~41 ± 5 nm. Since the concentration of rare earths in the host lattice has a significant effect on the emission intensities of these upconversion phosphors, it is critical to ensure the uniform precipitation of rare earth dopants (i.e., Y, Yb, and Er). No difference was observed in elemental composition measured using EDX for $NaYF_4$:Yb-Er synthesized with and without the addition of surfactants (Figure 3). Thus, the presence of the surfactants did not have a deleterious effect on the homogeneous

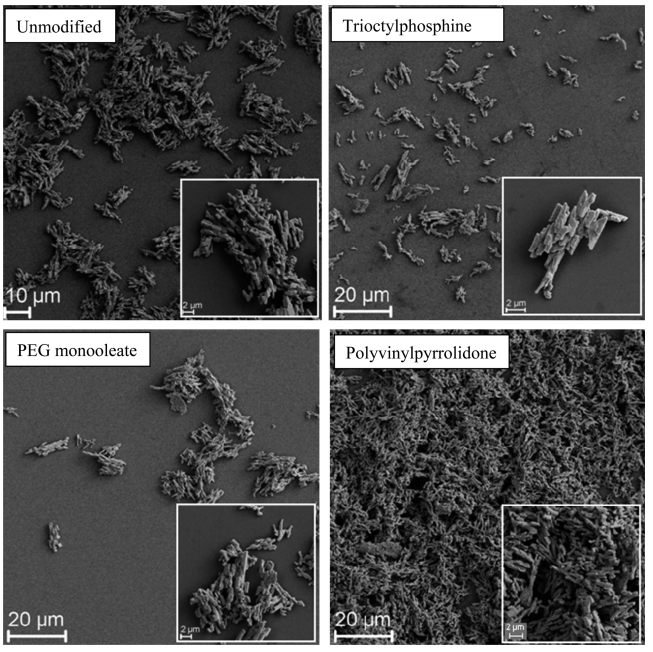

Figure 4. SEM micrographs of $NaYF_4$:Yb-Er particles synthesized with different surface capping agents compared with the unmodified particles. Distributions of major axis of particle sizes for unmodified, trioctylphosphine-, PEG monooleate-, and polyvinylpyrrolidone-modified particles were 2.74 ± 0.56, 2.20 ± 0.72, 2.81 ± 0.69, and 2.37 ± 0.59 μm, respectively. Distributions of minor axis of particle sizes for unmodified, trioctylphosphine-, PEG monooleate-, and polyvinylpyrrolidone-modified particles were 0.74 ± 0.19, 0.78 ± 0.17, 0.86 ± 0.12, and 0.76 ± 0.24 μm, respectively.

nucleation, growth and aging of particles from solution. SEM micrographs show that irregular, elongated micrometer-sized $NaYF_4$:Yb-Er particles were prepared using the different surfactants (Figure 4). No difference in particle morphology was observed for the $NaYF_4$:Yb-Er particles synthesized with and without the addition of surfactants. No statistically significant difference in particle sizes was observed for all $NaYF_4$:Yb-Er particles synthesized with and without the addition of surfactants, as shown by the size distribution (major and minor axis) stated in the caption of Figure 4. Broad particle size distributions were obtained in all cases, where the range of particles' lengths and widths were ~2−4 and ~0.5−0.9 μm, respectively. Since particle size, particle size distribution, crystallite size and morphology were not observed to be significantly different, we concluded that the surfactants did not play a dominant role in controlling the mechanisms for particle formation. Furthermore, the difference in particle sizes and crystallite sizes indicates that polycrystalline $NaYF_4$:Yb-Er particles were synthesized.

The surface areas of as-synthesized particles were estimated to be ~0.4−0.7 m^2/g, by assuming particle rod morphologies and density of 4.23 g/cm^3 (i.e., hexagonal-phase $NaYF_4$). On the basis of theoretical calculations, ~6×10^{-7} wt% of surfactants was estimated to be adsorbed on the particles, by taking into consideration a 10 nm thick surfactant coating and surfactant density of 1.2 g/cm^3. The low surface area and surfactant content led to difficulties in obtaining Fourier transform infrared spectra of the surface-modified particles to identify the adsorbed surfactant, and quantifying the adsorbed surfactant amount using thermal gravimetric methods. Therefore, the presence of the surfactants on as-synthesized $NaYF_4$:Yb-Er was evaluated using the XPS

Table 1. XPS Data Showing Surface Hydrocarbon Content for As-Synthesized Particles[a]

	unmodified		trioctylphosphine		PEG monooleate		polyvinylpyrrolidone	
element (at %/Na at %)	0 min	15 min	0 min	15 min	0 min	15 min	0 min	15 min
Y (3d)	0.91		0.96		0.91		0.85	
Yb (4d) Er (4d)	0.26		0.29		0.32		0.23	
C (1s)	5.25	4.02	7.66	3.17	7.49	4.39	10.23	3.54
Na (2s)	1.00	1.00	1.00	1.00	1.00	1.00	1.00	1.00

[a] The estimated standard deviation for composition (at%) is ~20% of measured average value.

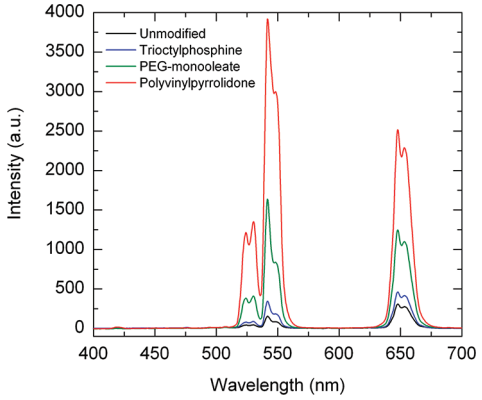

Figure 5. Effects of surface capping agents on infrared-to-visible upconversion emissions of as-synthesized $NaYF_4$:Yb-Er particles.

Table 2. Optical Efficiency of 550 nm Emission Using an Incident Power of 0.330 mW for the 975 nm Excitation[a]

	emitted power (nW)	optical efficiency (%)
unmodified	6	0.00182
trioctylphosphine	16	0.00485
PEG monooleate	23	0.00697
polyvinylpyrrolidone	35	0.01061

[a] The estimated standard deviation for emitted power is ~20%.

techniques (Table 1). For the unmodified particles, ~5 at%/Na at% of carbon was observed. The carbon that was detected on the unmodified particles was from residual environmental carbon sources (e.g., dust, residual organics, adhesive) that was either in the chamber or on the sample. The increased carbon content of ~8−10 at%/Na at% on the surface modified $NaYF_4$:Yb-Er compared to unmodified $NaYF_4$:Yb-Er particles verified the presence of the surfactants on the particles. The carbon content was reduced to ~3−4.5 at%/Na at% after the removal of the surface layers by sputtering the sample in Ar for ~15 min. Therefore, the surfactants were most likely coated on the surfaces of as-synthesized $NaYF_4$:Yb-Er particles. Considering that the decomposition or boiling temperatures were 250, 260, and 290 °C for polyvinylpyrrolidone, PEG monooleate, and trioctylphosphine, respectively, it was unlikely that these surfactants were degraded during the hydrothermal synthesis of $NaYF_4$:Yb-Er particles. In addition, the Y:(Yb+Er) atomic ratios of ~0.91:0.26 = 3.5:1 determined from the XPS results in Table 1 were consistent with atomic ratios of ~0.78:0.22 = 3.5:1 determined using EDX in Figure 3. The actual concentration of Y, Yb and Er normalized to Na is probably between that of the EDX and XPS measurements, since

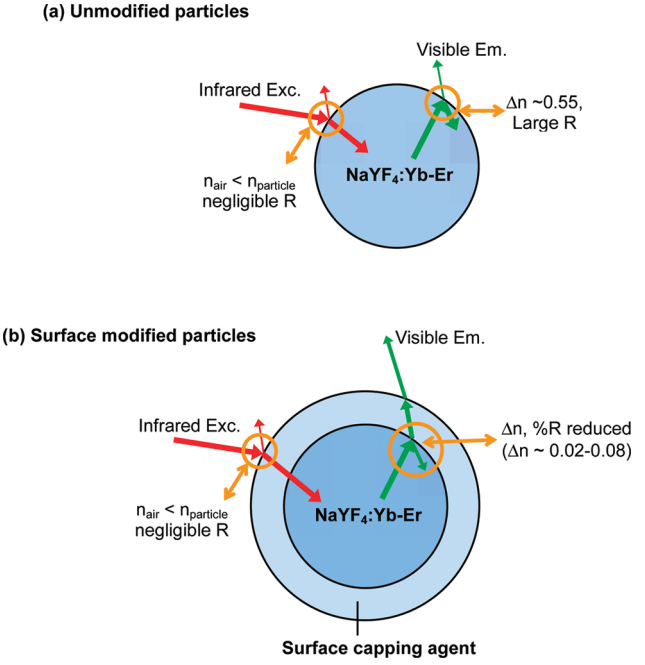

Figure 6. Schematic representation of reducing reflectance losses by reducing refractive index mismatches with surface capping agents.

the depth of penetration and principles of each analysis method are different. The XPS and EDX results indicated that the rare earth cations were uniformly distributed within the $NaYF_4$ microparticles.

The upconversion emission spectra of various surface-modified $NaYF_4$:Yb-Er particles as dried powders were collected. Several difficulties were encountered during the collection of particles suspended in various liquids (e.g., water, isopropanol). The rapid settling of the micrometer-sized particles in solution and large scattering losses from both the liquid medium and large particle sizes led to many inconsistencies in the emission spectra collected from the particle suspensions. Therefore, the upconversion emission spectra of dry $NaYF_4$:Yb-Er powders were measured. Figure 5 shows the upconversion emission spectra of the various surface-modified $NaYF_4$:Yb-Er particles. Distinct differences in emission intensities of as-synthesized $NaYF_4$:Yb-Er powders were observed. All surface modified particles were found to have more intense emissions than the unmodified $NaYF_4$:Yb-Er particles. Polyvinylpyrrolidone-modified $NaYF_4$:Yb-Er particles exhibited the most intense emissions. The ranking for the emission intensities was polyvinylpyrrolidone > PEG monooleate > trioctylphosphine > unmodified phosphor particles. The upconversion performance of these phosphors was subsequently quantified and evaluated by measuring the optical

Table 3. Reflectance Loss (From Back Reflections) at Interface Due to Refractive Index Mismatch

	refractive index, n	$n_1 - n_2$	reflectance (%)
unmodified (air)	1.000	0.550	4.652
trioctylphosphine	1.468	0.082	0.074
PEG monooleate	1.476	0.074	0.060
polyvinylpyrrolidone	1.530	0.020	0.004
$NaYF_4$	1.550		

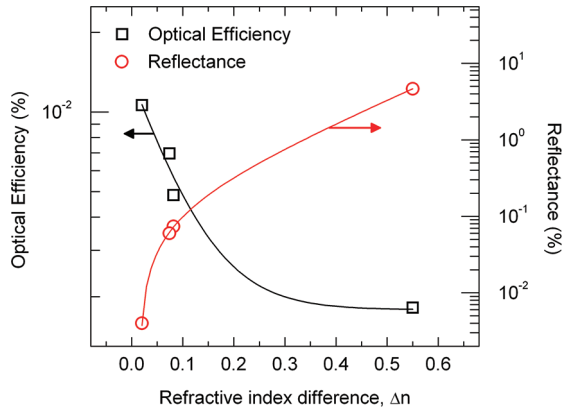

Figure 7. Optical efficiency and reflectance as a function of refractive index difference, Δn.

efficiency of the 550 nm emission (Table 2). The measured values were in the same order of magnitude to that of the radiant efficiency values of 10^{-3} to 10^{-4} that were previously reported for upconversion phosphors.[14,15] The polyvinylpyrrolidone-modified $NaYF_4$:Yb-Er particles were found to be ~5 times more efficient and brighter than the unmodified particles. Furthermore, the ranking in the optical efficiencies was consistent with observations made from the emission spectra in Figure 5.

Surface quenching effects from surfactant chemical functional groups (e.g., $-CH_2$, $-OH$) and surface defects were unlikely to contribute to differences in optical efficiency given the small specific surface area and large particle sizes. Therefore, the differences in optical efficiencies for the different surface-modified $NaYF_4$:Yb-Er particles were attributed to the reduction in reflectance losses at the particle−air interface. Fresnel reflection (i.e., principle for total internal reflection) occurs at any medium boundary where the refractive index changes from low to high, resulting in a portion of light being reflected back (see Figure 6). The reflectance loss of the incident infrared excitation light was negligible since the refractive index of air is less than that of $NaYF_4$:Yb-Er phosphor particles. The reflectance at the boundary, R, can be estimated using the following equation.

$$R(\%) = \frac{(n_1 - n_2)^2}{(n_1 + n_2)^2} \times 100\%$$

where n_1 and n_2 are the refractive indices of the core light-emitting $NaYF_4$:Yb-Er phosphor particles and surrounding medium (i.e., air or surface capping agents), respectively.[29−31] The refractive indices of the adsorbed surfactants were assumed to be the same as the surfactants in bulk form.

The large refractive index mismatch between the core $NaYF_4$:Yb-Er and surrounding medium leads to high reflectance losses of the emitted light (Table 3 and Figure 7). The portion of emitted light that is back reflected is most likely reabsorbed. While some of the reabsorbed light is re-emitted, another fraction of the reabsorbed portion is lost through either lower photon energy or nonradiative emissions. Consequently, the high reflectance loss leads to significant reduction of emitted light from the light-emitting $NaYF_4$:Yb-Er core particles. Consequently, the reduction of emitted light from the as-synthesized unmodified $NaYF_4$:Yb-Er powders results in lower measured optical efficiency values (Table 2 and Figure 7). The reflectance losses are lowered by reducing the refractive index mismatch between the core $NaYF_4$:Yb-Er particles and surrounding medium through the use of surfactants (Table 3). The gradual reduction in refractive index mismatches using surfactants across the particle surface−air interface has reduced the reflectance and reabsorption losses of emitted light. The reduced losses ultimately increase the optical efficiencies for surface-modified $NaYF_4$:Yb-Er particles (Table 2 and Figure 7).

4. CONCLUSIONS

Surfactants were adsorbed onto hydrothermally synthesized polycrystalline, hexagonal-phase $NaYF_4$:Yb-Er particles. The use of different surface capping agents was found to significantly change the optical efficiency of as-synthesized $NaYF_4$:Yb-Er particles. The polyvinylpyrrolidone-modified $NaYF_4$:Yb-Er particles were found to be ~5 times more efficient and brighter than the unmodified particles. The brightness and efficiency ranking was polyvinylpyrrolidone > PEG monooleate > trioctylphosphine > unmodified particles. The difference in efficiency was attributed to reduced reflectance losses at the boundary by reducing the refractive index mismatch between the core $NaYF_4$ particles and air using polyvinylpyrrolidone as a surface coating agent.

AUTHOR INFORMATION

Corresponding Author

*E-mail: riman@rci.rutgers.edu.

ACKNOWLEDGMENT

The authors thank the Defense Advanced Research Projects Agency (ONR-N00014-08-1-0131) for funding this research. We also acknowledge the technical assistance of Dr. B. Yakshinskiy with the XPS experiments.

REFERENCES

(1) Phillips, M. L. F.; Hehlen, M. P.; Nguyen, K.; Sheldon, J. M.; Cockroft, N. J. *Proc. Electrochem. Soc.* **2000**, *99−40*, 123–129.
(2) Scheps, R. *Prog. Quantum Electron.* **1996**, *20*, 271–358.
(3) Rapaport, A.; Milliez, J.; Bass, M.; Cassanho, A.; Jenssen, H. *J. Display Technol.* **2006**, *2*, 68–78.
(4) Hoeppe, H. A. *Angew. Chem., Int. Ed.* **2009**, *48*, 3572–3582.
(5) Eliseeva, S. V.; Bünzli, J-C. G. *Chem. Soc. Rev.* **2010**, *39*, 189–227.
(6) Naczynski, D. J.; Andelman, T.; Pal, D.; Chen, S.; Riman, R. E.; Roth, C. M.; Moghe, P. V. *Small* **2010**, *6*, 1631–1640.
(7) Tan, M. C.; Kumar, G. A.; Riman, R. E.; Brik, M. G.; Brown, E.; Hommerich, U. *J. Appl. Phys.* **2009**, *106*, 063118/1–063118/12.
(8) Kumar, G. A.; Chen, C. W.; Ballato, J.; Riman, R. E. *Chem. Mater.* **2007**, *19*, 1523–1528.
(9) Yi, G.-S.; Chow, G. M. *Adv. Funct. Mater.* **2006**, *16*, 2324–2329.
(10) Yi, G.-S.; Chow, G.-M. *J. Mater. Chem.* **2005**, *15*, 4460–4464.
(11) Wang, Q.; Tan, M. C.; Zhuo, R.; Kumar, G. A.; Riman, R. E. *J. Nanosci. Nanotechnol.* **2010**, *10*, 1685–1692.

(12) Aebischer, A.; Hostettler, M.; Hauser, J.; Krämer, K.; Weber, T.; Güdel, H. U.; Bürgi, H.-B. *Angew. Chem., Int. Ed.* **2006**, *45*, 2802–2806.
(13) Lage, M. M.; Matinaga, F. M.; Gesland, J.-Y.; Moreira, R. L. *J. Appl. Phys.* **2006**, *99*, 053510–053510/7.
(14) Bril, A.; Sommerdijk, J. L.; de Jager, A. W. *J. Electrochem. Soc.* **1975**, *122*, 660–663.
(15) Auzel, F.; Pecile, D. *J. Lumin.* **1973**, *8*, 32–43.
(16) Tan, M. C.; Connolly, J.; Riman, R. E. *J. Phys. Chem.* **2011**, *115*, 17952−17957.
(17) Yan, Z.-G.; Yan, C.-H. *J. Mater. Chem.* **2008**, *18*, 5046–5059.
(18) Li, C.; Yang, J.; Quan, Z.; Yang, P.; Kong, D.; Lin, J. *Chem. Mater.* **2007**, *19*, 4933–4942.
(19) He, F.; Yang, P.; Wang, D.; Niu, N.; Gai, S.; Li, X. *Inorg. Chem.* **2011**, *50*, 4116–4124.
(20) Wang, F.; Wang, J.; Liu, X. *Angew. Chem., Int. Ed.* **2010**, *49*, 7456–7460.
(21) Boyer, J.-C.; Manseau, M.-P.; Murray, J. I.; van Veggel, F. C. J. M. *Langmuir* **2010**, *26*, 1157–1164.
(22) Carenco, S.; Le Goff, X. F.; Shi, J.; Roiban, L.; Ersen, O.; Boissière, C.; Sanchez, C.; Mezailles, N. *Chem. Mater.* **2011**, *23*, 2270–2277.
(23) Liu, Y.; Wang, C.; Wei, Y.; Zhu, L.; Li, D.; Jiang, J. S.; Markovic, N. M.; Stamenkovic, V. R.; Sun, S. *Nano Lett.* **2011**, *11*, 1614–1617.
(24) Boyer, J. C.; Johnson, N. J. J.; van Veggel, F. C. J. M. *Chem. Mater.* **2009**, *21*, 2010–2012.
(25) Schmidt, H.; Kropf, C.; Schiestel, T.; Schirra, H.; Sepeur, S.; Lesniak, C. *Ceram. Trans.* **1998**, *95*, 49–64.
(26) Kumar, S.; Sharma, N.; Verma, N. K.; Chakarvarti, S. K. *J. Adv. Mater. Optoelectron.* **2007**, *1*, 677–682.
(27) Lee, S.; Jeong, S.; Kim, D.; Hwang, S.; Jeon, M.; Moon, J. *Superlattices Microstruct.* **2008**, *43*, 330–339.
(28) Rasband, W. S. IMAGEJ; U.S. National Institutes of Health: Bethesda, 1997; http://rsb.info.nih.gov/ij.
(29) Zhengwen, Y.; Zhu, K.; Song, Z.; Yu, X.; Zhou, D.; Yin, Z.; Yan, L.; Jianbei, Q. *Appl. Phys. A: Mater. Sci. Process.* **2011**, *103*, 995–999.
(30) http://www.chemnet.com/dict/dict--31943-11-0--en.html, accessed Jan 2011.
(31) http://www.texloc.com/closet/cl_refractiveindex.html, accessed Jan 2011.